Author for correspondence:
Julián F. Hillyer
e-mail: julian.hillyer@vanderbilt.edu

THE ROYAL SOCIETY
PUBLISHING

The immune deficiency and c-Jun N-terminal kinase pathways drive the functional integration of the immune and circulatory systems of mosquitoes

Yan Yan[1,†], Leah T. Sigle[1,†], David C. Rinker[1], Tania Y. Estévez-Lao[1], John A. Capra[1,2] and Julián F. Hillyer[1]

[1]Department of Biological Sciences, Vanderbilt University, Nashville, TN, USA
[2]Bakar Computational Health Sciences Institute and Department of Epidemiology and Biostatistics, University of California San Francisco, San Francisco, CA, USA

JFH, 0000-0002-3178-0201

The immune and circulatory systems of animals are functionally integrated. In mammals, the spleen and lymph nodes filter and destroy microbes circulating in the blood and lymph, respectively. In insects, immune cells that surround the heart valves (ostia), called periostial haemocytes, destroy pathogens in the areas of the body that experience the swiftest haemolymph (blood) flow. An infection recruits additional periostial haemocytes, amplifying heart-associated immune responses. Although the structural mechanics of periostial haemocyte aggregation have been defined, the genetic factors that regulate this process remain less understood. Here, we conducted RNA sequencing in the African malaria mosquito, *Anopheles gambiae*, and discovered that an infection upregulates multiple components of the immune deficiency (IMD) and c-Jun N-terminal kinase (JNK) pathways in the heart with periostial haemocytes. This upregulation is greater in the heart with periostial haemocytes than in the circulating haemocytes or the entire abdomen. RNA interference-based knockdown then showed that the IMD and JNK pathways drive periostial haemocyte aggregation and alter phagocytosis and melanization on the heart, thereby demonstrating that these pathways regulate the functional integration between the immune and circulatory systems. Understanding how insects fight infection lays the foundation for novel strategies that could protect beneficial insects and harm detrimental ones.

1. Introduction

Insect immune cells, called haemocytes, produce pattern recognition receptors that detect microbial invaders, activate immune signalling pathways, and kill pathogens via phagocytosis, lysis, melanization and other mechanisms [1–3]. These haemocytes exist in a dynamic body cavity called the haemocoel, where the flow of haemolymph constantly circulates them throughout the body. However, not all haemocytes circulate; one quarter of haemocytes are attached to tissues and remain sessile [4]. A sub-population of these sessile haemocytes concentrates on the outer surface of the heart and, more specifically, in the regions surrounding heart valves called ostia [5,6]. These heart-associated haemocytes, called periostial haemocytes, reside in the locations of the body that experience the highest haemolymph flow, and intensely phagocytose bacteria and malaria parasites within seconds of their entry into the haemocoel. As this is happening, additional haemocytes leave circulation and aggregate in the periostial regions of the heart, thereby augmenting the heart-associated immune response [5,6]. Although the kinetics and structural mechanics of periostial immunity have only been described in the African malaria mosquito,

Anopheles gambiae [5–9], heart-associated immune responses have also been reported in other mosquito species, fruit flies, stick insects and moths [10–12]. Further analysis of insects from 16 different orders showed that the functional integration between the immune and circulatory systems is conserved across the entire insect lineage [13].

In mosquitoes, pattern recognition receptors in the thioester-containing protein family, together with adhesion and phagocytosis factors in the Nimrod protein family, positively regulate immune responses on the heart [14,15]. However, heart-associated immune responses are triggered by both bacterial and malarial infections, and by both peptidoglycan and B-1,3-glucan [5,6]. Hence, the regulatory networks that drive periostial haemocyte aggregation undoubtedly extend beyond pattern recognition receptors and adhesion molecules. In insects, immune responses are primarily driven by pathways such as Toll, immune deficiency (IMD), c-Jun N-terminal kinase (JNK) and Jak/Stat [1,16]. The Toll pathway acts via the transcription factor Rel1, and primarily responds to Gram(+) bacteria, fungi and rodent malaria parasites, whereas the IMD and interlinked JNK pathways act via the transcription factors Rel2 and JNK, respectively, and primarily respond to Gram(–) bacteria and human malaria parasites [17,18]. In fruit flies, the Toll pathway is also involved in haemocyte differentiation, and its constitutive activation disrupts sessile haemocytes [19,20]. The IMD pathway has not been directly linked to cellular immunity but its canonical activator, the peptidoglycan recognition protein PGRP-LC, positively regulates phagocytosis of *Escherichia coli* but not *Staphylococcus aureus* [21]. The Jak/Stat pathway acts via the Stat family of transcription factors. In mosquitoes, this pathway responds to malaria parasites and viruses [22,23], and in fruit flies, it controls haemocyte maturation and differentiation [24,25].

The goal of this study was to identify genes and regulatory pathways that drive periostial haemocyte aggregation in *A. gambiae*. Using an unbiased RNA sequencing (RNAseq) approach that was followed by empirical testing with RNA interference (RNAi), we uncovered that the IMD and JNK pathways drive periostial haemocyte aggregation and immune responses on the heart, thereby regulating the functional integration between the immune and circulatory systems of mosquitoes.

2. Results

2.1. Infection upregulates immune genes in periostial haemocytes

To identify genes that may drive periostial haemocyte aggregation, we undertook an unbiased RNAseq approach where we sequenced the transcriptome of tissues from mosquitoes that were naive, injured or infected with Gram(–) GFP-*E. coli* or Gram(+) *S. aureus* (figure 1*a*,*b*; electronic supplementary material, dataset S1). Three tissues were isolated at 4 h after treatment: (i) the heart containing periostial haemocytes, (ii) the haemolymph containing circulating haemocytes and (iii) the entire abdomen. Mosquitoes were assayed at 4 h after treatment because the number of periostial haemocytes approximately doubles within the first hour of infection, and plateaus by 4 h after infection [5]. In these experiments, most mosquitoes were used for sequencing, but a subset of mosquitoes was used to confirm that infection induces heart-

associated cellular immune responses. Indeed, a resident population of periostial haemocytes was present in both naive and injured mosquitoes, and the number of periostial haemocytes increased 1.8- and 1.6-fold after GFP-*E. coli* and *S. aureus* infection, respectively (figure 1*b*,*c*).

RNAseq revealed that, relative to the heart and periostial haemocytes of naive and injured mosquitoes, 73 and 132 genes are upregulated more than fourfold ($p < 0.05$) in the heart and periostial haemocytes of mosquitoes infected with GFP-*E. coli* and *S. aureus*, respectively (figure 1*d*). Because periostial haemocyte aggregation is a dynamic immune response that occurs during any bacterial infection, we hypothesized that its core molecular drivers must be preferentially upregulated in periostial haemocytes following both *E. coli* and *S. aureus* infection. We found that 55 genes met this overlap criterion (figure 1*e*; electronic supplementary material, table S1). Comparing the heart and periostial haemocyte RNAseq data to RNAseq data from (i) circulating haemocytes and (ii) the entire abdomen then revealed that infection upregulates more genes in the heart with periostial haemocytes than in the circulating haemocytes or the abdomen (figure 1*d–e*; electronic supplementary material, tables S1–S3).

We then scrutinized the reported or predicted function of the 55 candidate genes. Twelve have immune function (figure 1*f*), and strikingly, six are part of IMD and JNK pathway: the peptidoglycan recognition protein *PGRP-LA* [26], the inhibitor of apoptosis family member *IAP2* [27], the IMD pathway transcription factor *rel2* [28,29], the antimicrobial peptides *cec3* [29] and *def1* [30,31] and the JNK pathway transcription factor *JNK3* [32,33]. Multiple aspects of the IMD and JNK pathway are represented: upstream components such as *PGRP-LA* and *IAP2*, and downstream elements from both branches of the pathway, with the classical IMD cascade represented by *rel2*, *cec3* and *def1*, and the bifurcation into the JNK pathway represented by *JNK3* [27,34,35] (electronic supplementary material, figure S1). Relevant to this finding, activating the IMD pathway induces the expression of the scavenger and phagocytosis receptor *eater* [36], which positively regulates haemocyte adhesion in fruit flies and periostial haemocyte aggregation in mosquitoes [15,37]. The IMD pathway also induces the expression of the thioester containing protein *TEP1*, which is involved in phagocytosis and periostial haemocyte aggregation [14]. Moreover, transglutaminases are pleiotropic enzymes that in *Drosophila* inhibit the IMD pathway [38,39], and a mosquito transglutaminase—*TGase3*—negatively regulates periostial haemocyte aggregation and has infection-dependent effects on the heart rate [40,41]. Finally, the JNK pathway is associated with cell adhesion and phagocytosis by regulating the cytoskeleton [32,42]. The JNK pathway also induces the expression of the engulfment receptor *draper* [43] and *TEP1* [33], both of which affect periostial haemocyte aggregation in mosquitoes [14,15]. All six IMD and JNK pathway genes identified in our unbiased screen were more highly upregulated in the heart and periostial haemocytes than in the other tissues (electronic supplementary material, figure S2). The remaining six candidate genes with immune function that were identified in our screen—*CLIPB17*, *DDC*, *SRPN16*, *CLIPB11*, *PGRP-LB* and *upd3a*—do not participate in a common pathway.

Because the downregulation of genes could also impact haemocyte aggregation, we assessed the genes that were downregulated after both *E. coli* and *S. aureus* infection, relative to naive and injured mosquitoes. No genes met this
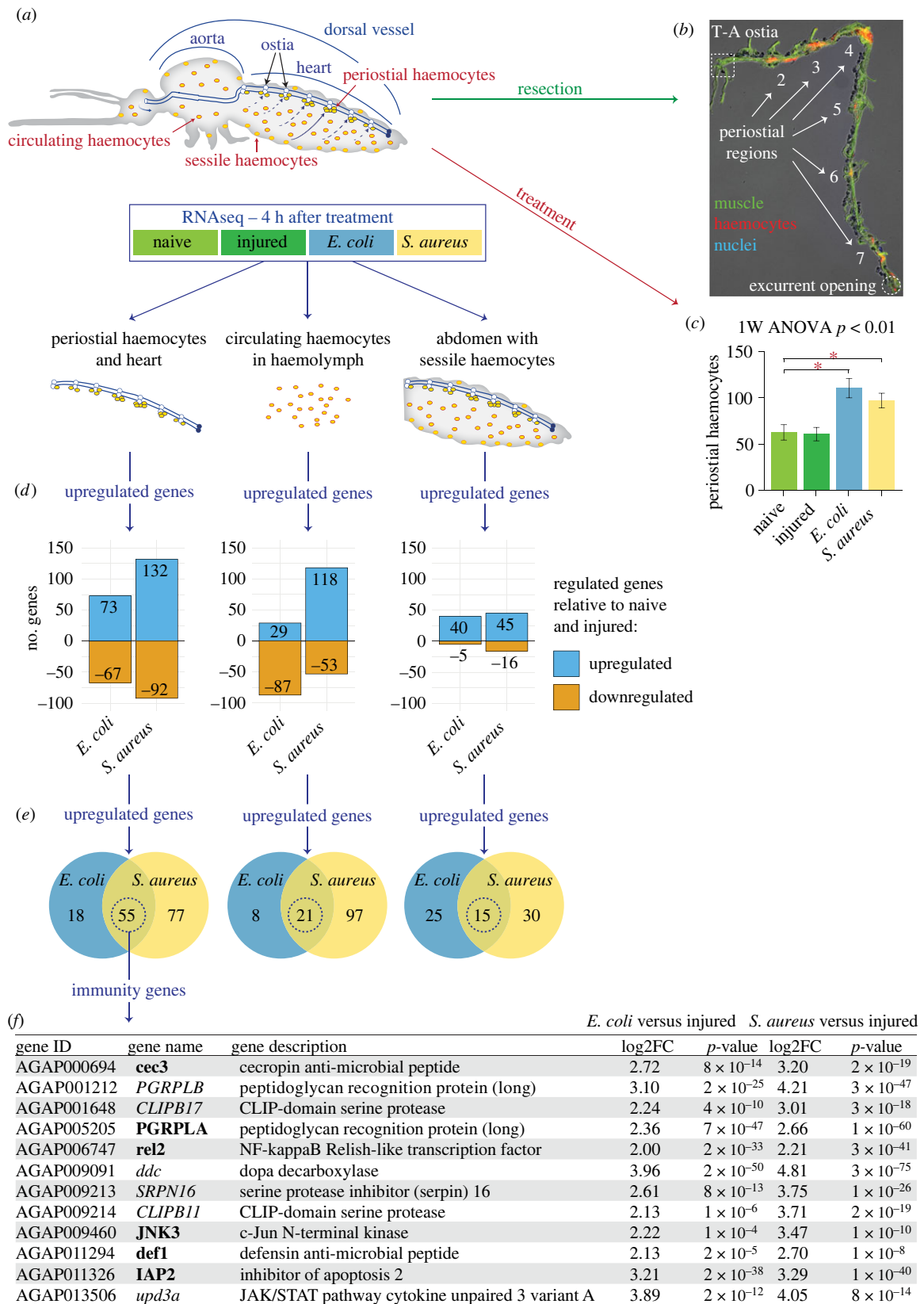
Figure 1. Infection upregulates immune genes in periostial haemocytes. (*a*) The heart with periostial haemocytes, the circulating haemocytes and the abdomen of mosquitoes that were naive, injured or infected with GFP-*E. coli* or *S. aureus* were sequenced by RNAseq at 4 h post-treatment. (*b*) Fluorescence and DIC overlay shows that the periostial haemocytes (CM-Dil; red) remain attached to a resected heart (phalloidin; green). Marked are the periostial regions for each abdominal segment, the thoraco-abdominal (T-A) ostia and the posterior excurrent opening. Image is modified from Sigle & Hillyer [7], and reproduced according to Creative Commons Attribution License CC BY. (*c*) Naive and injured mosquitoes have resident periostial haemocytes, but infection for 4 h with GFP-*E. coli* or *S. aureus* induces the aggregation of additional haemocytes at the periostial regions. Whiskers show the standard error of the mean (s.e.m.; $n = 14$ for all groups). (*d*) Bar plots show the number of genes significantly upregulated or downregulated at 4 h after GFP-*E. coli* or *S. aureus* infection in the periostial haemocytes and heart (left), the circulating haemocytes (middle) and the entire abdomen (right). (*e*) Venn diagrams show that 55, 21 and 15 genes are significantly upregulated in the periostial haemocytes, the circulating haemocytes or the abdomen, respectively, during both GFP-*E. coli* and *S. aureus* infections. (*f*) Table listing the immune genes that are among the 55 genes that were upregulated in the heart with periostial haemocytes following both GFP-*E. coli* or *S. aureus* infection. Genes that participate in the IMD and JNK pathway are in bold.
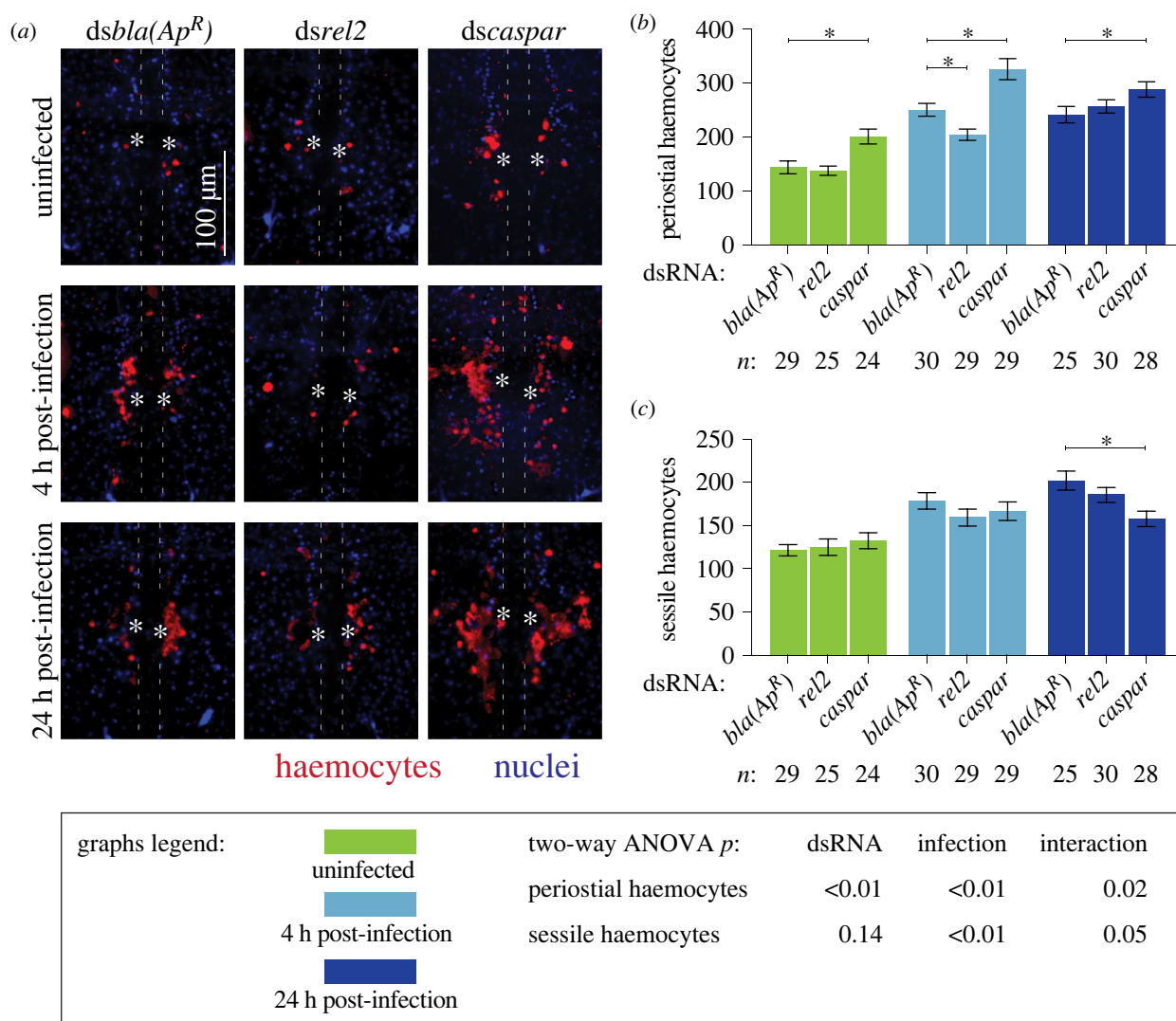
Figure 2. The IMD pathway drives periostial haemocyte aggregation. (a) Fluorescence images show periostial haemocytes (CM-Dil; red) surrounding a single pair of ostia (asterisks) on a segment of the heart (outlined by dotted lines) of ds*bla(Ap^R)*, ds*rel2* and ds*caspar* mosquitoes that were not infected or had been infected with GFP-*E. coli* for 4 or 24 h. Anterior is on top. (b,c) Graphs for ds*bla(Ap^R)*, ds*rel2* and ds*caspar* mosquitoes that were not infected or had been infected with GFP-*E. coli* for 4 or 24 h. The graphs show: (b) average number of periostial haemocytes; and (c) average number of sessile haemocytes outside of the periostial regions in the tergum of abdominal segments 4 and 5. Graphs show the mean and s.e.m. The data were analysed by two-way ANOVA (bottom box), followed by Dunnett's multiple comparison test. *n* indicates sample size. Asterisks in graphs indicate *post hoc p* < 0.05.

criterion for the abdomen, but 29 genes met this criterion for the heart with periostial haemocytes and 19 genes for the circulating haemocytes (electronic supplementary material, tables S4 and S5). Five of these genes were shared between the heart with periostial haemocytes and the circulating haemocytes, but none of the 43 genes have a classical role in immunity or carry a function suggestive of involvement in haemocyte aggregation. Therefore, based on the RNAseq analyses, we hypothesized that the main driver of periostial haemocyte aggregation is the IMD and JNK pathway.

2.2. The IMD pathway positively regulates periostial haemocyte aggregation

To determine whether the IMD pathway regulates periostial haemocyte aggregation, we synthesized double-stranded RNA (dsRNA) to target the IMD cascade transcription factor, *rel2*, and its negative regulator, *caspar*, and achieved RNAi-based silencing of 43% and 37%, respectively, compared to the ds*bla(Ap^R)* control mosquitoes (electronic supplementary

material, figure S3). Moreover, because *Tep1* is (i) activated by the Rel2 arm of the IMD pathway [44,45] and (ii) a positive driver of periostial haemocyte aggregation [14], we measured its mRNA abundance in *rel2* and *caspar* RNAi mosquitoes. Silencing of *rel2* did not alter *TEP1* mRNA abundance but silencing of *caspar* increased it. Because *cec3* and *def1* are also activated by Rel2 [29–31], we measured their mRNA abundance in RNAi mosquitoes. Silencing of *rel2* decreased *cec3* and *def1* mRNA abundance whereas silencing of *caspar* increased them (electronic supplementary material, figure S3). Overall, these data are consistent with the role that the Rel2 arm of the IMD pathway plays in regulating *TEP1*, *cec3* and *def1* expression.

To assess whether the IMD pathway drives heart-associated immune responses, we compared the number and activity of periostial haemocytes in *rel2* and *caspar* RNAi mosquitoes, relative to ds*bla(Ap^R)* control mosquitoes (figures 2 and 3). As expected, infection for 4 h induced the aggregation of haemocytes at the periostial regions of ds*bla(Ap^R)* mosquitoes, and this aggregation remained in place at 24 h. In uninfected mosquitoes, knocking down *rel2* did not change
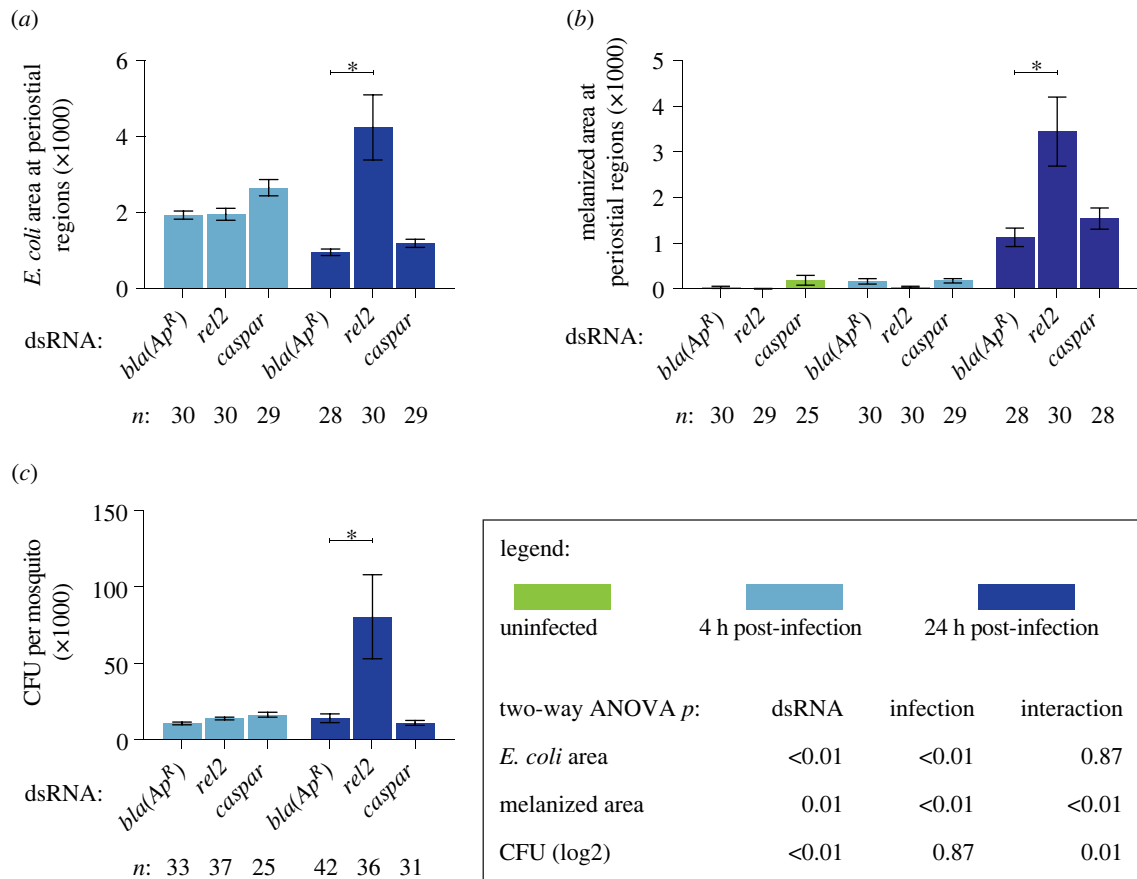
Figure 3. The IMD pathway modulates immune responses on the heart and the systemic antimicrobial response. (*a–c*) Graphs for ds*bla(Ap^R)*, ds*rel2* and ds*caspar* mosquitoes that were not infected or had been infected with GFP-*E. coli* for 4 or 24 h. The graphs show: (*a*) pixel area of GFP-*E. coli* in the periostial regions; (*b*) pixel area of melanin in the periostial regions; and (*c*) the systemic GFP-*E. coli* infection intensity. Graphs show the mean and s.e.m. The data were analysed by two-way ANOVA (bottom box), followed by Dunnett's multiple comparison test. *n* indicates sample size. Asterisks in graphs indicate *post hoc p* < 0.05.

the number of periostial haemocytes, but at 4 h following infection, knockdown of *rel2* decreased the number of periostial haemocytes by 18%, relative to ds*bla(Ap^R)* mosquitoes (figure 2*a,b*). At 24 h post-infection, the effect of *rel2* RNAi on periostial haemocyte aggregation was diminished. When we instead knocked down *caspar*, the number of periostial haemocytes increased by 39% in uninfected mosquitoes, and infection for 4 and 24 h increased the number of periostial haemocytes by 30% and 19%, respectively, relative to similarly treated ds*bla(Ap^R)* mosquitoes. This shows that *rel2* positively regulates periostial haemocyte aggregation whereas *caspar* negatively regulates this process.

To determine whether the IMD pathway specifically affects periostial haemocytes and not sessile haemocytes in general, we counted the number of sessile haemocytes outside of the periostial regions in the tergum of abdominal segments 4 and 5 in the same mosquitoes examined for periostial haemocytes (figure 2*c*). Knockdown of *rel2* or *caspar* did not alter the number of non-periostial sessile haemocytes in uninfected mosquitoes or mosquitoes infected for 4 h. However, at 24 h following infection, *caspar* RNAi decreased non-periostial sessile haemocytes by 22%. These results demonstrate that the IMD pathway regulates periostial haemocyte aggregation while having a minimal effect on the rest of the sessile haemocytes.

Periostial haemocytes phagocytose bacteria, leading to their accumulation at the periostial regions [5,6]. To determine whether the IMD pathway affects the phagocytic activity of periostial haemocytes, we measured the GFP-*E. coli*

fluorescence pixel area in the periostial regions of infected mosquitoes (figure 3*a*; electronic supplementary material, figure S4). At 4 h following infection, the GFP-*E. coli* pixel area was similar regardless of dsRNA treatment. At 24 h after infection, this area decreased in ds*bla(Ap^R)* and ds*caspar* mosquitoes, indicating that periostial haemocytes efficiently destroyed the pathogens. However, at 24 h following infection, *rel2* RNAi significantly increased GFP-*E. coli* accumulation at the periostial regions. Periostial haemocytes also phagocytose melanized bacteria [5,6], and one melanization related-gene— dopa decarboxylase or *DDC* [46,47]—was upregulated in both the heart with periostial haemocytes and the circulating haemocytes. Therefore, we measured melanin accumulation in the periostial regions (figure 3*b*; electronic supplementary material, figure S4). Melanin was absent in uninfected mosquitoes and mosquitoes that were infected for 4 h. However, at 24 h following infection, *rel2* RNAi increased melanin deposits at the periostial regions whereas *caspar* RNAi had no effect.

The increased accumulation of GFP-*E. coli* and melanin in *rel2* RNAi mosquitoes at 24 h after infection could be due to either (i) enhanced phagocytosis by periostial haemocytes or (ii) higher bacterial proliferation in the haemocoel, which places increased pressure on the phagocytosis response. To differentiate between these two scenarios, we measured the systemic GFP-*E. coli* infection intensity and observed that, at 4 h after infection, the bacterial intensity was similar for all dsRNA treatments, but at 24 h, knockdown of *rel2* resulted in a higher infection intensity than treatment with ds*caspar* or ds*bla(Ap^R)* (figure 3*c*). This suggests that *rel2* is essential for

proper bacterial killing in the haemocoel, and therefore, knocking it down increases infection intensity in a manner that leads to increased phagocytosis in the periostial regions. However, because silencing *rel2* and *caspar* had opposite effects on periostial haemocyte aggregation at 4 h, a time when dsRNA treatment does not impact infection intensity, we conclude that the IMD pathway is a positive regulator of periostial haemocyte aggregation.

PGRP-LC is the canonical activator of the IMD pathway [1], but PGRP-LA (i) activates the IMD pathway in the midgut of mosquitoes and in the barrier epithelia of fruit flies [26,48], (ii) is expressed in *Drosophila* haemocytes [49] and (iii) is upregulated in the heart and periostial haemocytes (figure 1*f*). Therefore, we tested the involvement of PGRP-LA in periostial haemocyte aggregation. *PGRP-LA* has three splice forms, so to knock it down, we synthesized ds*PGRP-LA-RARB* to target the *RA* and *RB* splice forms, and ds*PGRP-LA-RC* to target the *RC* splice form. Using these dsRNAs, we achieved RNAi-based silencing that ranged from 56% to 77%, compared to the ds*bla(Ap^R)* control mosquitoes (electronic supplementary material, figure S5). *PGRP-LA* knockdown with any dsRNA did not alter the number of periostial haemocytes, the number of non-periostial sessile haemocytes, melanin accumulation at the periostial regions or systemic infection intensity (electronic supplementary material, figure S6). However, knockdown of *PGRP-LA-RC* increased phagocytosis of GFP-*E. coli* in the periostial regions, which suggests that the RC splice form is involved in the phagocytosis response (electronic supplementary material, figure S6).

2.3. The JNK pathway positively regulates periostial haemocyte aggregation

We next tested whether the JNK pathway regulates periostial haemocyte aggregation. *Anopheles gambiae* encodes two JNK genes: *JNK1* and *JNK3* [50]. Therefore, we synthesized dsRNA to target the JNK cascade transcription factors, *JNK1* and *JNK3*, and their negative regulator, *puckered* (*puc*). Because of high sequence identity between *JNK1* and *JNK3*, ds*JNK1/3* simultaneously targeted both JNK genes. RNAi-based knockdown resulted in 33%, 44% and 31% reduction in mRNA abundance of *JNK1*, *JNK3* and *puc*, respectively (electronic supplementary material, figure S7). Moreover, because the JNK pathway has also been implicated in the expression of *TEP1* [51], we measured the mRNA abundance of *TEP1*, *cec3* and *def1* in *JNK1/JNK3* and *puc* RNAi mosquitoes. Manipulating the JNK pathway did not have a clear impact on effector gene expression (electronic supplementary material, figure S7). The lack of clarity on how the JNK pathway controls the expression of *TEP1*, *cec3* or *def1* could be due to their co-regulation by other pathways, or a consequence of incomplete gene silencing of *JNK1/3* and *puc*.

To assess whether the JNK pathway drives heart-associated immune responses, we compared the number and activity of periostial haemocytes in *JNK1/3* and *puc* RNAi mosquitoes, relative to ds*bla(Ap^R)* control mosquitoes (figures 4 and 5). Regardless of infection status, the number of periostial haemocytes was statistically similar between ds*JNK1/3* and ds*bla(Ap^R)* mosquitoes, although ds*JNK1/3* mosquitoes averaged fewer periostial haemocytes than control mosquitoes for all treatments (figure 4*a,b*). Knockdown of *puc*, however, increased the number of periostial

haemocytes 1.6-fold in uninfected mosquitoes, and 1.4- and 1.5-fold at 4 and 24 h following GFP-*E. coli* infection, respectively, relative to similarly treated ds*bla(Ap^R)* mosquitoes. To further determine whether *puc* specifically affects periostial haemocytes or sessile haemocytes in general, we quantified the number of non-periostial sessile haemocytes on the tergum of the same mosquitoes (figure 4*c*). *JNK1/3* RNAi mosquitoes showed a trend of fewer non-periostial sessile haemocytes than control mosquitoes regardless of infection status. Treatment with ds*puc*, however, increased the number of non-periostial sessile haemocytes for all treatments. This demonstrates that the JNK pathway positively regulates both periostial and non-periostial sessile haemocyte abundance.

We next measured whether the JNK pathway affects the phagocytic activity of periostial haemocytes (figure 5*a*; electronic supplementary material, figure S8). At 4 h following infection, the GFP-*E. coli* pixel area was similar regardless of dsRNA treatment. However, at 24 h following infection, periostial haemocytes in ds*puc* mosquitoes phagocytosed more GFP-*E. coli* than the ds*bla(Ap^R)* mosquitoes. We then quantified the melanized bacteria that were sequestered by periostial haemocytes (figure 5*b*; electronic supplementary material, figure S8). Melanin deposits were undetectable in uninfected mosquitoes and mosquitoes at 4 h post infection; however, at 24 h following GFP-*E. coli* infection, more melanin was present in ds*puc* mosquitoes than in ds*bla(Ap^R)* controls.

The difference in GFP-*E. coli* and melanin accumulation in ds*puc* mosquitoes could be due to (i) enhanced phagocytosis by periostial haemocytes or (ii) higher bacterial proliferation in the haemocoel. To differentiate between these two scenarios, we quantified the systemic *E. coli* infection intensity and found that the bacterial intensity was similar regardless of dsRNA treatment (figure 5*c*). Therefore, this suggests that *puc* negatively regulates haemocyte adhesion and phagocytic activity, and demonstrates that the JNK pathway is a positive regulator of periostial immune responses.

3. Discussion

Previous microarray and RNAseq analyses revealed genes and signalling pathways that are active in mosquito haemocytes [52–58], including those that are activated in specific subpopulations of haemocytes [59–61]. However, these studies only focused on circulating haemocytes, and therefore, failed to capture the biology of sessile haemocytes. Yet, one quarter of haemocytes are sessile [4], and they play significant roles in haematopoiesis [62,63], wound healing [64], and pathogen killing [9,65,66]. Therefore, extrapolating the molecular signatures of circulating haemocytes to those of sessile haemocytes likely misses the essential factors that make sessile haemocytes conduct their specific immune activities. Periostial haemocytes are a subpopulation of sessile haemocytes that reside on the heart, where they sequester and kill pathogens in areas of high haemolymph flow [5,6,13]. To better understand how an infection drives the migration of haemocytes to the heart and how these immune cells kill pathogens at the periostial regions, we sequenced the periostial haemocyte transcriptome and discovered that the IMD and JNK pathway drives periostial immune responses (figure 6).
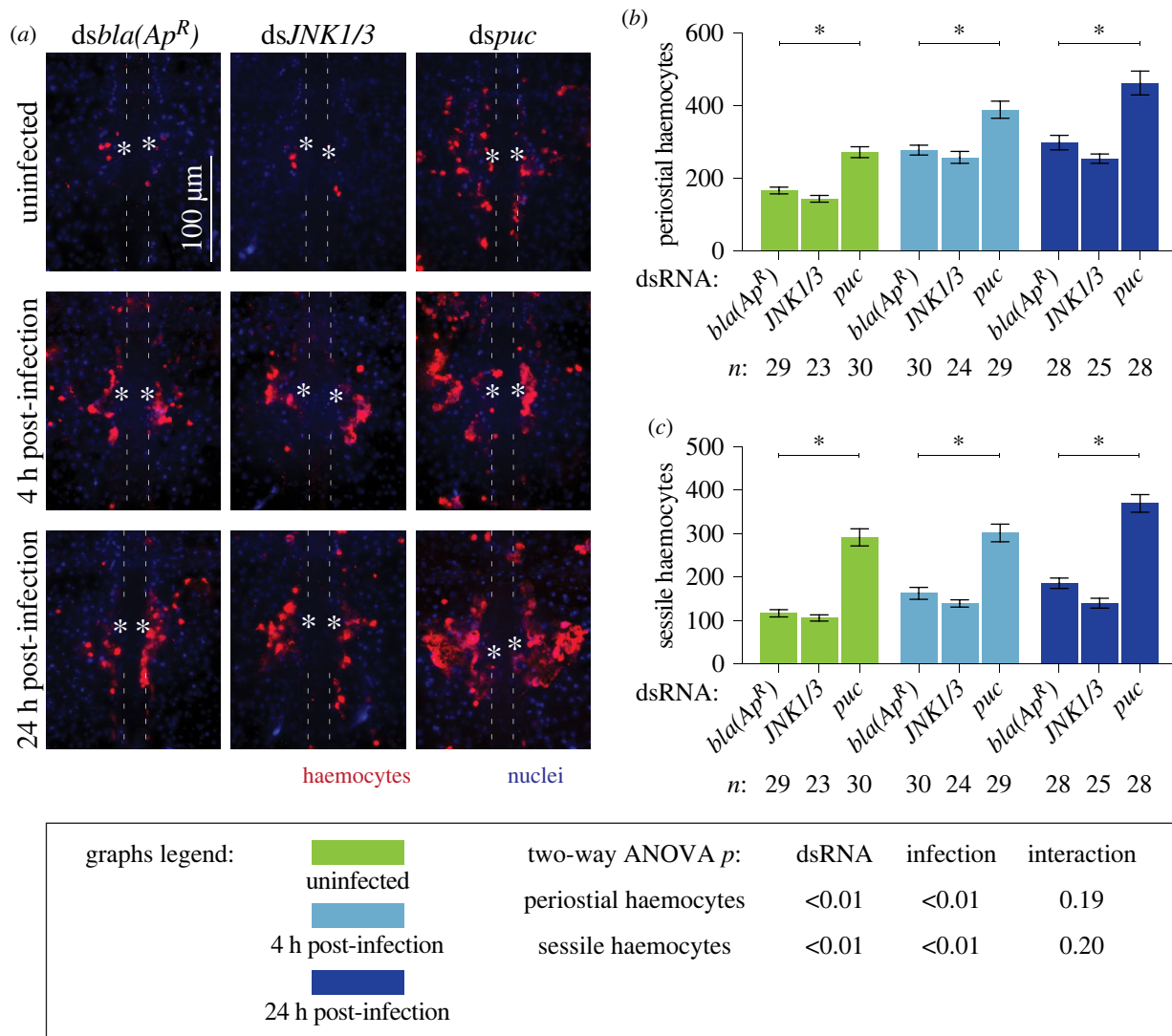
Figure 4. The JNK pathway drives periostial haemocyte aggregation. (*a*) Fluorescence images show periostial haemocytes (CM-Dil; red) surrounding a single pair of ostia (asterisks) on a segment of the heart (outlined by dotted lines) of ds*bla(Ap^R)*, ds*JNK1/3* and ds*puc* mosquitoes that were not infected or had been infected with GFP-*E. coli* for 4 or 24 h. Anterior is on top. (*b,c*) Graphs for ds*bla(Ap^R)*, ds*JNK1/3* and ds*puc* mosquitoes that were not infected or had been infected with GFP-*E. coli* for 4 or 24 h. The graphs show: (*b*) average number of periostial haemocytes; and (*c*) average number of sessile haemocytes outside of the periostial regions in the tergum of abdominal segments 4 and 5. Graphs show the mean and s.e.m. The data were analysed by two-way ANOVA (bottom box), followed by Dunnett's multiple comparison test. *n* indicates sample size. Asterisks in graphs indicate *post hoc* $p < 0.05$.

The IMD pathway controls the production of anti-microbial peptides [1,27], but here we show that the IMD pathway also regulates a cellular immune response: the transition of haemocytes from a circulating to a sessile state on the heart. Specifically, knockdown of the positive regulator of the IMD pathway, *rel2*, decreases infection-induced periostial haemocyte aggregation, whereas knockdown of the negative regulator of the IMD pathway, *caspar*, increases the number of periostial haemocytes. We hypothesize that the IMD pathway drives periostial haemocyte aggregation via two cascades that are also driving phagocytosis: the TEP1-TEP3-LRP1-CED6L and TEP4-BINT2-CED2L-CED5L pathways [67]. The IMD pathway induces the expression of *TEP1* and *TEP4* [30,31,68], and both of these genes positively regulate periostial haemocyte aggregation [14]. Moreover, two downstream molecules—the low-density-lipoprotein-receptor-related protein LRP1 and the beta integrin BINT2—are transmembrane proteins that in mammals and insects have overlapping functions in phagocytosis and adhesion [69–71], and therefore, likely facilitate the adhesion of haemocytes to the heart. In this study, we also confirmed

the positive role that REL2 plays in pathogen killing [29,44,68,72–78]. When we systemically knocked down the expression of *rel2*, bacteria proliferated uncontrollably during the later stages of infection. We hypothesize that knocking down *rel2* initially suppresses periostial haemocyte aggregation, but as the infection progresses and the intensity increases, the necessity of periostial immune responses also increases, and this pressure recruits haemocytes to the heart and enhances their collective phagocytic activity. Overall, our data show that the IMD pathway drives periostial haemocyte aggregation during the early stages of infection and limits systemic infection intensity during the later stages of infection.

The JNK pathway modulates mosquito longevity, regulates oviposition, and limits infection with malaria parasites and viruses [33,51,79–82]. Here, we found that overexpressing the JNK pathway by knocking down the negative regulator, *puc*, increases the number of periostial and adjacent sessile haemocytes. This suggests that the JNK pathway positively regulates haemocyte adhesion. Indeed, the *Drosophila* orthologue of mosquito *JNK1* and *JNK3*, called *basket*, is involved in the formation of actin-rich and focal adhesion
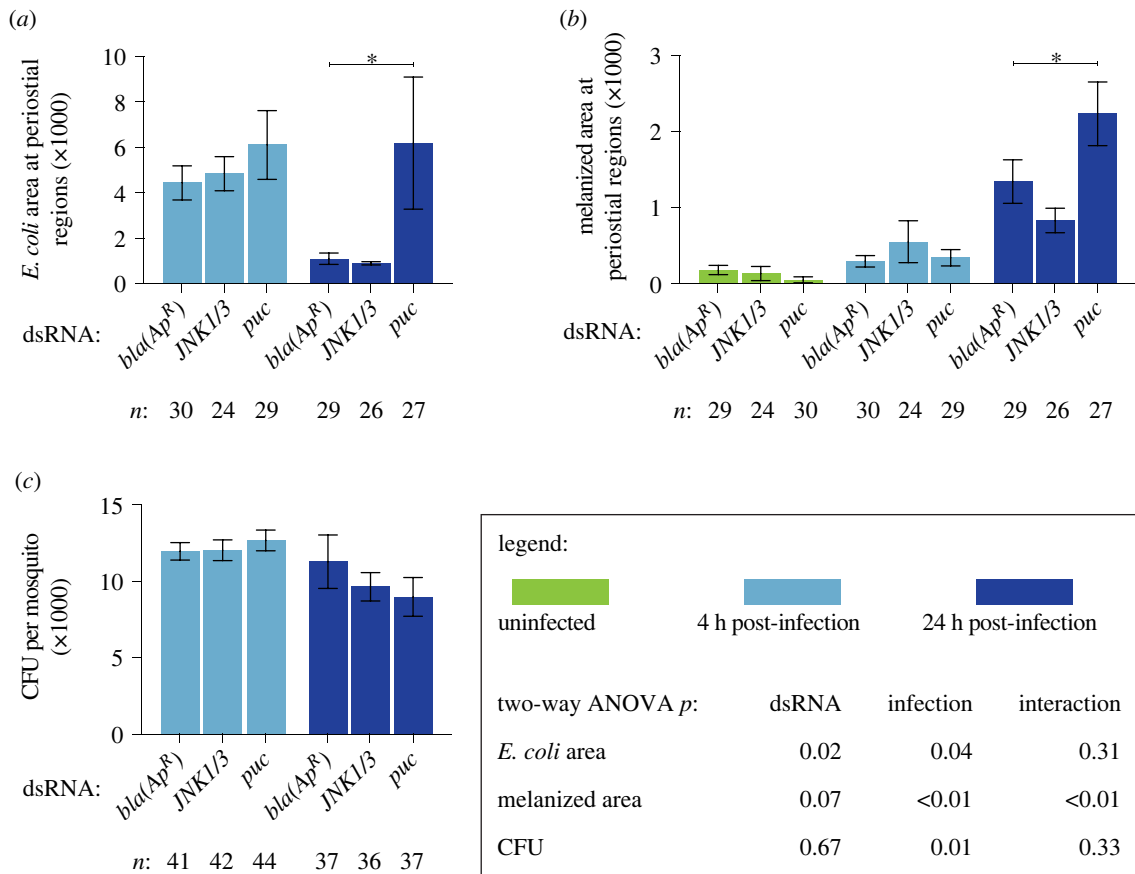
Figure 5. The JNK pathway modulates immune responses on the heart but not the systemic antimicrobial response. (a–c) Graphs for dsbla(Ap^R), dsJNK1/3 and dspuc mosquitoes that were not infected or had been infected with GFP-E. coli for 4 or 24 h. The graphs show: (a) pixel area of GFP-E. coli in the periostial regions; (b) pixel area of melanin in the periostial regions; and (c) the systemic GFP-E. coli infection intensity. Graphs show the mean and s.e.m. The data were analysed by two-way ANOVA (bottom box), followed by Dunnett's multiple comparison test. n indicates sample size. Asterisks in graphs indicate post hoc $p < 0.05$.
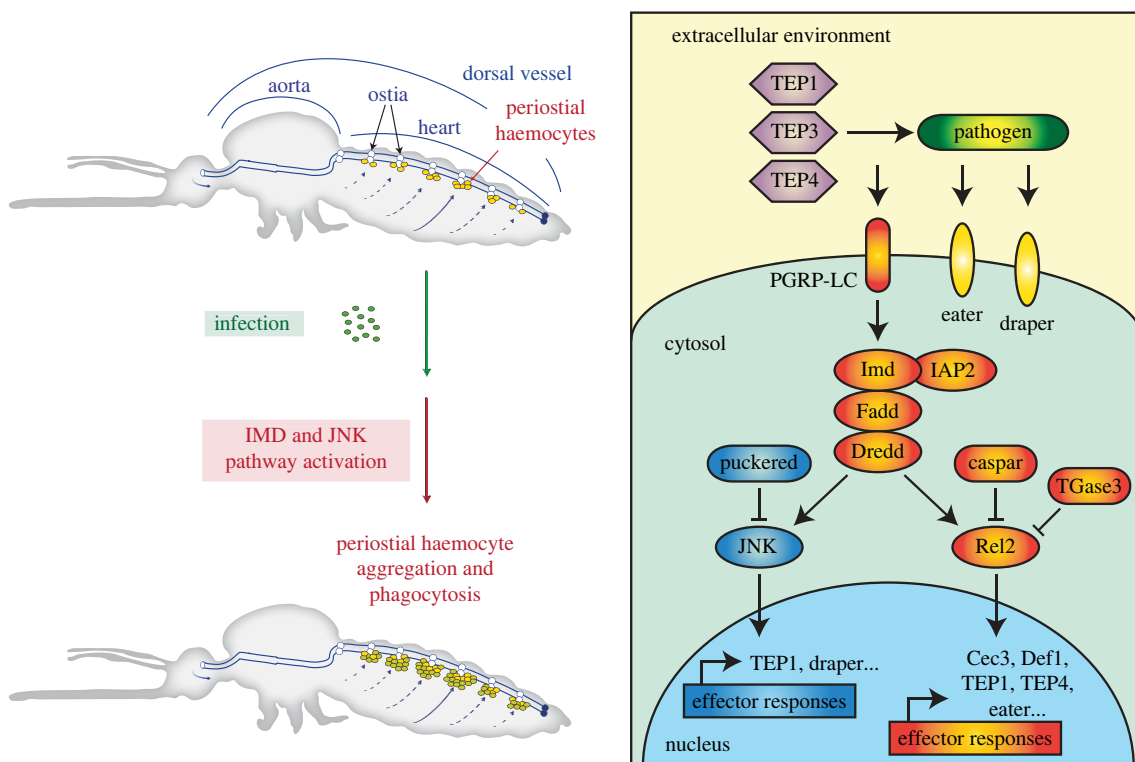

Figure 6. The IMD and JNK pathways, together with TEP proteins (TEP1, TEP3 and TEP4), Nimrod proteins (Draper and Eater) and a transglutaminase, regulate heart-associated immune responses in mosquitoes.

kinase-rich placodes in haemocytes [83]. The JNK pathway also induces haemocyte differentiation in *Drosophila*, producing large lamellocytes that adhere and encapsulate parasitoid eggs [84]. We found that overactivating the JNK pathway does not alter infection intensity in mosquitoes, but it increases the accumulation of *E. coli* and melanin on the heart, suggesting that the JNK pathway positively regulates the phagocytosis and melanization responses. Indeed, JNK1 positively regulates melanization in mosquitoes that are refractory to malaria [51], and overexpressing the JNK pathway in aphids increases the melanin-producing activity of phenoloxidase and the phagocytic activity of haemocytes [85]. We hypothesize that the JNK pathway regulates phagocytosis by periostial haemocytes in a manner that involves two proteins already known to be involved in periostial haemocyte aggregation: TEP1 and draper [14,15]. The JNK pathway activates the expression of both of these genes [33,80,86], and TEP1 opsonizes pathogens for phagocytosis whereas draper activates phagocytic processes [14,15,67,87–89]. In our study, we could not distinguish between the roles that *JNK1* and *JNK3* play in periostial haemocyte aggregation. However, simultaneous knockdown of both resulted in phenotypes that were opposite of *puc* knockdown, strongly suggesting that JNK1 or JNK3—or both—positively regulates periostial haemocyte aggregation.

Because both the IMD and JNK pathways induce the production of *TEP1* [30,33,68,80], we hypothesize that they share the TEP1-TEP3-LRP1-CED6L phagocytosis cascade that leads to haemocyte aggregation. However, we also hypothesize that the IMD and JNK pathways use additional, independent mechanisms to regulate periostial haemocyte aggregation for three reasons. First, even though the two pathways share upstream signalling molecules, they bifurcate and activate their own set of effector genes [34,35]. Second, knocking down the components of the IMD and JNK pathways resulted in different phenotypes, especially for periostial and non-periostial sessile haemocytes. Third, in *Drosophila*, draper and the BINT2 orthologue (Integrin *βv*) function independently [90], and in mosquitoes, draper is regulated by the JNK pathway whereas BINT2 is involved in the IMD-regulated and TEP4-mediated phagocytosis cascade [31,67,70,86].

Bacteria, malaria parasites and fungal components all induce periostial haemocyte aggregation, and this process is structurally conserved across the entire insect lineage [5,6,13]. Therefore, it is likely that other proteins contribute to this process. Indeed, infection also induces the upregulation of *upd3a* by periostial haemocytes, which is a ligand for the receptor of the JAK/STAT pathway [91]. The Toll pathway also induces haemocyte proliferation [92,93] and the expression of *TEP1* [44], which positively regulates periostial haemocyte aggregation [14]. Beyond immune pathways, periostial haemocyte aggregation may also be under the influence of neuronal and hormonal control. For example, injecting mosquitoes with the neuropeptide, allatotropin, increases the number of periostial and non-periostial sessile haemocytes [94]. Therefore, the regulation of periostial haemocyte aggregation is not expected to be limited to the IMD and JNK pathways.

To date, we have tested the involvement of several haemocyte-produced factors on periostial haemocyte aggregation. However, the heart itself may produce complementary factors that drive this immune response. For example, a fibroblast growth factor is highly regulated in the heart and periostial haemocytes. Its orthologue in *Drosophila*, called *Branchless*, is expressed in the heart and pericardial cells, and regulates haemocyte differentiation in the lymph glands of the larval heart [95,96]. Moreover, reducing the expression of the *Drosophila* cardiac extracellular matrix (ECM) proteins, *Pericardin* and *Laminin A*, disrupts the formation of the cardiac ECM and lowers the number of haemocytes on the heart [12,97]. These data suggest that the heart and its associated structures facilitate the binding of circulating haemocytes to the periostial regions.

The mosquito genome encodes three transglutaminase genes, and our RNAseq experiment revealed that two of them are upregulated in the heart and periostial haemocytes following infection. In *Drosophila*, transglutaminase negatively regulates the IMD pathway by (i) crosslinking the transcription factor, Relish, into a polymer and (ii) incorporating natural primary amines into the DNA binding site of Relish [38,39]. We recently tested whether transglutaminases are involved in periostial responses in *A. gambiae*, and found that *TGase3*—but not *TGase1* or *TGase2*—negatively regulates periostial haemocyte aggregation during the early stages of infection and the sequestration of melanin by periostial haemocytes during the later stages of infection [40]. Moreover, disrupting *TGase2* and *TGase3* has infection-dependent effects on the heart rate [41]. Combined, these data further support our conclusion that the IMD pathway is a positive driver of heart-associated immune responses (figure 6).

Heart-associated immune responses occur in insects from at least 16 different taxonomic orders, including insects that are of agricultural, urban and medical importance [13]. Understanding the genetic factors that drive periostial haemocyte aggregation in *A. gambiae* sheds light on how this medically important insect and other insects of societal importance fight the pathogens that invade them. Indeed, the TEP gene family, the Nimrod gene family (Eater, Nimrod and Draper) and the JNK pathway are conserved amongst insects [50,98–100], and although some insects in the order Hemiptera lack components of the IMD pathway, all insects queried to date still have a functional IMD-based immune response [101–104]. Therefore, we conclude that the IMD and JNK pathways, together with TEP and Nimrod proteins, are primary regulators of the heart-associated immune responses in insects.

4. Material and methods

4.1. Mosquitoes, bacteria, infection and replication

Anopheles gambiae, Giles *sensu stricto* (G3; Diptera: Culicidae), were maintained at 27°C, 75% relative humidity, and a 12 h : 12 h light : dark photoperiod [105]. Experiments were done using female adults fed 10% sucrose. After any treatment, mosquitoes of a given treatment were housed together, returned to the environmental chamber, and given access to 10% sucrose. Tetracycline resistant, GFP-expressing *E. coli* (modified DH5α; GFP-*E. coli*) and *S. aureus* (RN6390) were grown in Luria-Bertani (LB) and tryptic soy broth, respectively, at 37°C in a shaking incubator. Dilutions of the bacterial cultures were injected at the thoracic anepisternal cleft using a Nanoject III (Drummond Scientific Company, Broomall, PA, USA). The infection dose was determined by plating the cultures and counting the colony forming units (CFUs).

In this study, a biological replicate is an independent experiment that uses mosquitoes from an independent egg

batch. A technical replicate is an experimental resampling of a biological replicate. All data collected were included in the analysis; no data were excluded.

4.2. RNAseq: treatment, tissue collection, RNA isolation and library preparation

Six-day-old mosquitoes were randomly divided into four groups: (i) naive (unmanipulated), (ii) injured by injecting 69 nl of sterile LB, (iii) infected by injecting 69 nl of GFP-E. coli (approx. 75 779 CFUs) and (iv) infected by injecting 69 nl of S. aureus (approx. 39 451 CFUs). At 4 h after treatment, three tissues were isolated: (i) the heart with periostial haemocytes, (ii) haemolymph with circulating haemocytes and (iii) the entire abdomen containing all its internal organs and tissues (i.e. gut, ovaries, epidermis, muscles, ventral nerve cord and other tissues). To isolate the heart, mosquitoes were bisected along the coronal plane in RNase-free PBS, and the heart with the periostial haemocytes was resected by severing the alary muscles and detaching it from the cuticle [7]. To isolate circulating haemocytes, haemolymph was perfused by making an incision in the last abdominal segment, injecting RNase-free PBS into the haemocoel through the cervical membrane, and collecting the first two drops that exited the abdomen [106]. The abdomens were isolated by bisecting mosquitoes on the transverse plane along the thoraco-abdominal junction.

To isolate RNA from hearts or abdomens, samples were homogenized in TRIzol Reagent (Invitrogen, Carlsbad, CA, USA), extracted following the TRIzol protocol, and resuspended in Buffer RLT (Qiagen, Hilden, Germany) with 2% 2-mercaptoethanol. The RNA was further purified using the RNeasy Micro Kit (Qiagen), DNase treated, and eluted in RNase-free water. To isolate RNA from circulating haemocytes, perfused haemolymph was collected in Buffer RLT and 2% 2-mercaptoethanol, and RNA was isolated using the RNeasy Micro Kit as above.

No a priori statistical method was used to pre-determine sample sizes. The number of RNAseq samples and biological replicates was determined prior to the initiation of the study, and was based on our determination that three biological replicates is a conservative approach to detect statistical differences (if any) in gene expression. Three biological replicates were conducted; each heart sample contained 72 hearts, each haemolymph sample contained perfusate from 108 mosquitoes, and each abdomen sample contained 36 abdomens.

The integrity and quantity of RNA was assessed on a 2100 Bioanalyzer (Agilent Technologies, Santa Clara, CA, USA) using an RNA 6000 Series II Nano kit for abdomen samples and a Pico kit for the heart and haemolymph samples. The library for sequencing was prepared using 1 µg of RNA and the NEBNext Ultra kit (New England BioLabs, Ipswich, MA, USA), according to the protocol for low-input samples. Library quality and concentration were assessed using a DNA 1000 Series II kit on the 2100 Bioanalyzer.

4.3. RNAseq: Illumina sequencing and differential gene expression analysis

All 36 samples—four treatments, three tissue types and three biological replicates—were sequenced across three lanes on an Illumina HiSeq 3000 (paired-end, 75 base pair read) at Vanderbilt University's Vantage facility. Reads were mapped to the A. gambiae genome (AgamP4.7) by STAR [107,108]. The number of uniquely mapped reads per sample averaged 23 698 077 (range: 18 487 153–31 487 002), which represented 94.03% of the total reads in a sample. Differential expression was calculated based on reads per kilobase per million by DESeq2 [109]. Genes were considered significantly regulated at $\log_2$ fold change ≥ 2 or $\log_2$ fold change ≤ -2 and the Benjamini–Hochberg adjusted $p < 0.05$. RNAseq results are presented in electronic supplementary material, dataset S1, which includes read counts and log2 fold changes. Using four-fold expression difference as the criterion, together with experimental replication and statistical validation, is a conservative approach that is proven to yield accurate and reliable results [110]. RNAseq data were deposited into NCBI (https://www.ncbi.nlm.nih.gov) as SRA data PRJNA730047.

4.4. Double-stranded RNA synthesis and RNA interference

Double-stranded RNA was synthesized for rel2, caspar, PGRP-LA, JNK1 and JNK3, and puc. Anopheles gambiae cDNA was amplified by PCR using gene-specific primers with T7 promoter tags (electronic supplementary material, table S6). dsRNA was synthesis using the MEGAscript T7 Kit (Applied Biosystems) as described [14,15]. As a negative control, dsRNA was synthesized for the non-mosquito gene, $bla(Ap^R)$, using DNA from E. coli BL21(DE3) containing the pET-46 plasmid as template (EMD Chemicals, Gibbstown, NJ) [14,15].

Two- or three-day-old mosquitoes were intrathoracically injected 300 ng of dsRNA to initiate systemic gene silencing. Four days later, mosquitoes were divided into two groups for phenotypic analyses: (i) uninfected and (ii) infected with GFP-E. coli (approx. 16 528 CFUs). Injured mosquitoes were not included in the experiments because injury does not induce periostial haemocyte aggregation [4–6]. RNAi efficiency of the targeted genes and mRNA abundance of the downstream effector genes TEP1, cec3 and def1 was determined by qPCR [14]. Briefly, RNA was isolated using TRIzol from 10 whole bodies for each time and treatment, purified, and used for cDNA synthesis using the SuperScript III First-Strand Synthesis System for RT-PCR (Invitrogen) as described [14,15]. qPCR was conducted using gene-specific primers (electronic supplementary material, table S6) and Power SYBR Green PCR Master Mix (Applied Biosystems, Foster City, CA, USA) on a Bio Rad CFX Connect Real-Time Detection System (Hercules, CA, USA). Relative quantification was conducted using the $2^{-\Delta\Delta C_T}$ method, with RpS7 as the reference and RpS17 as a control [111]. Two to three biological replicates were conducted per gene, and the value for each biological replicate is the average of two or three technical replicates.

4.5. Fluorescence labelling and mosquito dissection

Haemocytes were labelled with the Vybrant CM-DiI Cell-Labeling Solution (Invitrogen) as we described [5]. Briefly, live mosquitoes were injected approximately 0.4 µl of 67 µM CM-DiI and 1.08 mM Hoechst 33342 (nuclear stain; Invitrogen) in PBS, incubated at 27°C for 20 min, and injected 16% paraformaldehyde. Ten min later, abdomens were bisected along a coronal plane, and the dorsal portions containing the

heart and periostial haemocytes were mounted on glass slides using Aqua-Poly/Mount (Polysciences; Warrington, PA, USA). CM-DiI stains live haemocytes, and we have used this technique to monitor haemocyte location, number and migration, as well as haemocyte-mediated phagocytosis and melanization [4–9,13–15,40].

4.6. Microscopy and image acquisition

Specimens were imaged on a Nikon Eclipse Ni-E compound microscope connected to a Nikon Digital Sight DS-Qi1 camera and Advanced Research NIS Elements software (Nikon, Tokyo, Japan). Z-stacks for bright field, red fluorescence (haemocytes), green fluorescence (GFP-*E. coli*) and blue fluorescence (nuclei) were acquired using a linear encoded Z-motor. Specific channels were selected and all images within a stack were combined into a two-dimensional image using the extended depth of focus (EDF) function.

4.7. Quantification of haemocytes

Haemocytes, labelled with both CM-DiI and Hoechst 33342, were counted manually by examining all images within a Z-stack [14]. A cell was a periostial haemocyte if adjacent to an ostium, and a non-periostial sessile haemocyte if attached to the abdominal wall outside of a periostial region [4,5]. Periostial haemocytes were counted within abdominal segments 2–7 (all abdominal periostial regions) whereas non-periostial sessile haemocytes were only counted on the tergum of segments 4 and 5. Haemocytes were not counted on the aorta, the thoraco-abdominal ostia or the excurrent openings because few haemocytes are there, and infection does not induce aggregation at those locations [7,8]. Data were analysed by two-way ANOVA, followed by Dunnett's multiple comparison test, with ds*bla(Ap^R)* mosquitoes as the reference (Prism 9, GraphPad Software, San Diego, CA, USA). Data for RNAi phenotypic experiments are from individual mosquitoes, which were sampled across three to four biological replicates. The exception is experiments for PGRP-LA, where mosquitoes were sampled across two biological replicates.

4.8. Quantification of GFP-*E. coli* and melanin at the periostial regions

In NIS-Elements, each periostial region in an EDF image was delineated using the ROI tool. GFP-*E. coli* at the periostial regions was calculated by measuring the area of pixels with intensities above a threshold that distinguished GFP-*E. coli* from background fluorescence [14]. Melanin was quantified by measuring the area of pixels with intensities below a threshold that distinguished dark melanized areas from non-melanized areas [14]. For each mosquito, measurements from all ROIs were added. Data were analysed by two-way ANOVA, followed by Dunnett's multiple comparison test, with ds*bla(Ap^R)* mosquitoes as the reference.

4.9. Quantification of bacterial infection intensity

Mosquitoes that were infected with tetracycline resistant GFP-*E. coli* for 4 or 24 h were homogenized individually in PBS. A dilution of the homogenate was spread on LB agar containing tetracycline, and plates were incubated overnight at 37°C. The CFUs were counted and used to calculate infection intensity. Data were analysed by two-way ANOVA, followed by Dunnett's multiple comparison test, with ds*bla(Ap^R)* mosquitoes as the reference. For *rel2* and *caspar* RNAi mosquitoes, data were first $\log_2$ transformed to achieve normality, and then analysed by two-way ANOVA.

References

1. Hillyer JF. 2016 Insect immunology and hematopoiesis. *Dev. Comp. Immunol.* **58**, 102–118. (doi:10.1016/j.dci.2015.12.006)

2. Strand M. 2008 The insect cellular immune response. *Insect Sci.* **15**, 1–14. (doi:10.1111/j.1744-7917.2008.00183.x)

3. Hillyer JF, Strand MR. 2014 Mosquito hemocyte-mediated immune responses. *Curr. Opin. Insect Sci.* **3**, 14–21. (doi:10.1016/j.cois.2014.07.002)

4. King JG, Hillyer JF. 2013 Spatial and temporal in vivo analysis of circulating and sessile immune cells in mosquitoes: hemocyte mitosis following infection. *BMC Biol.* **11**, 55. (doi:10.1186/1741-7007-11-55)

5. King JG, Hillyer JF. 2012 Infection-induced interaction between the mosquito circulatory and immune systems. *PLoS Pathog.* **8**, e1003058. (doi:10.1371/journal.ppat.1003058)

6. Sigle LT, Hillyer JF. 2016 Mosquito hemocytes preferentially aggregate and phagocytose pathogens in the periostial regions of the heart that experience the most hemolymph flow. *Dev. Comp. Immunol.* **55**, 90–101. (doi:10.1016/j.dci.2015.10.018)

7. Sigle LT, Hillyer JF. 2018 Mosquito hemocytes associate with circulatory structures that support intracardiac retrograde hemolymph flow. *Front Physiol.* **9**, 1187. (doi:10.3389/fphys.2018.01187)

8. Sigle LT, Hillyer JF. 2018 Structural and functional characterization of the contractile aorta and associated hemocytes of the mosquito *Anopheles gambiae*. *J. Exp. Biol.* **221**(Pt 12), jeb181107. (doi:10.1242/jeb.181107)

9. League GP, Hillyer JF. 2016 Functional integration of the circulatory, immune, and respiratory systems in

mosquito larvae: pathogen killing in the hemocyte-rich tracheal tufts. *BMC Biol.* **14**, 78. (doi:10.1186/s12915-016-0305-y)

10. Hernández-Martínez S, Lanz-Mendoza H, Martínez-Barnetche J, Rodríguez MH. 2013 Antimicrobial properties of *Anopheles albimanus* pericardial cells. *Cell Tissue Res.* **351**, 127–137. (doi:10.1007/s00441-012-1505-6)

11. da Silva R, da Silva SR, Lange AB. 2012 The regulation of cardiac activity by nitric oxide (NO) in the Vietnamese stick insect, *Baculum extradentatum*. *Cell. Signal.* **24**, 1344–1350. (doi:10.1016/j.cellsig.2012.01.010)

12. Ghosh S, Singh A, Mandal S, Mandal L. 2015 Active hematopoietic hubs in *Drosophila* adults generate hemocytes and contribute to immune response. *Dev. Cell.* **33**, 478–488. (doi:10.1016/j.devcel.2015.03.014)

13. Yan Y, Hillyer JF. 2020 The immune and circulatory systems are functionally integrated across insect evolution. *Sci. Adv.* **6**, eabb3164. (doi:10.1126/sciadv.abb3164)

14. Yan Y, Hillyer JF. 2019 Complement-like proteins TEP1, TEP3 and TEP4 are positive regulators of periostial hemocyte aggregation in the mosquito *Anopheles gambiae. Insect. Biochem. Mol. Biol.* **107**, 1–9. (doi:10.1016/j.ibmb.2019.01.007)

15. Sigle LT, Hillyer JF. 2018 *Eater* and *draper* are involved in the periostial haemocyte immune response in the mosquito *Anopheles gambiae. Insect. Mol. Biol.* **27**, 429–438. (doi:10.1111/imb.12383)

16. Zhang W, Tettamanti G, Bassal T, Heryanto C, Eleftherianos I, Mohamed A. 2021 Regulators and signalling in insect antimicrobial innate immunity: functional molecules and cellular pathways. *Cell. Signal.* **83**, 110003. (doi:10.1016/j.cellsig.2021.110003)

17. Shaw WR, Catteruccia F. 2019 Vector biology meets disease control: using basic research to fight vector-borne diseases. *Nat. Microbiol.* **4**, 20–34. (doi:10.1038/s41564-018-0214-7)

18. King JG. 2020 Developmental and comparative perspectives on mosquito immunity. *Dev. Comp. Immunol.* **103**, 103458. (doi:10.1016/j.dci.2019.103458)

19. Banerjee U, Girard JR, Goins LM, Spratford CM. 2019 *Drosophila* as a genetic model for hematopoiesis. *Genetics* **211**, 367–417. (doi:10.1534/genetics.118.300223)

20. Schmid MR *et al*. 2016 Genetic screen in *Drosophila* larvae links *ird1* function to Toll signaling in the fat body and hemocyte motility. *PLoS ONE* **11**, e0159473. (doi:10.1371/journal. pone.0159473)

21. Rämet M, Manfruelli P, Pearson A, Mathey-Prevot B, Ezekowitz RA. 2002 Functional genomic analysis of phagocytosis and identification of a *Drosophila* receptor for *E. coli. Nature* **416**, 644–648. (doi:10.1038/nature735)

22. Bahia AC *et al*. 2011 The JAK-STAT pathway controls *Plasmodium vivax* load in early stages of *Anopheles aquasalis* infection. *PLoS Negl. Trop. Dis.* **5**, e1317. (doi:10.1371/journal.pntd.0001317)

23. Souza-Neto JA, Sim S, Dimopoulos G. 2009 An evolutionary conserved function of the JAK-STAT pathway in anti-dengue defense. *Proc. Natl Acad. Sci. USA* **106**, 17 841–17 846. (doi:10.1073/pnas.0905006106)

24. Minakhina S, Tan W, Steward R. 2011 JAK/STAT and the GATA factor Pannier control hemocyte maturation and differentiation in *Drosophila. Dev. Biol.* **352**, 308–316. (doi:10.1016/j.ydbio.2011.01.035)

25. Krzemień J, Dubois L, Makki R, Meister M, Vincent A, Crozatier M. 2007 Control of blood cell homeostasis in *Drosophila* larvae by the posterior signalling centre. *Nature* **446**, 325–328. (doi:10.1038/nature05650)

26. Gendrin M, Turlure F, Rodgers FH, Cohuet A, Morlais I, Christophides GK. 2017 The peptidoglycan recognition proteins PGRPLA and PGRPLB regulate *Anopheles* immunity to bacteria and affect infection by *Plasmodium. J. Innate Immun.* **9**, 333–342. (doi:10.1159/000452797)

27. Myllymäki H, Valanne S, Rämet M. 2014 The *Drosophila* IMD signaling pathway. *J. Immunol.* **192**, 3455–3462. (doi:10.4049/jimmunol.1303309)

28. Garver LS, Bahia AC, Das S, Souza-Neto JA, Shiao J, Dong Y, Dimopoulos G. 2012 *Anopheles* Imd pathway factors and effectors in infection intensity-dependent anti-*Plasmodium* action. *PLoS Pathog.* **8**, e1002737. (doi:10.1371/journal.ppat.1002737)

29. Meister S *et al*. 2005 Immune signaling pathways regulating bacterial and malaria parasite infection of the mosquito *Anopheles gambiae. Proc. Natl Acad. Sci. USA* **102**, 11 420–11 425. (doi:10.1073/pnas.0504950102)

30. Garver LS, Dong Y, Dimopoulos G. 2009 Caspar controls resistance to *Plasmodium falciparum* in diverse anopheline species. *PLoS Pathog.* **5**, e1000335. (doi:10.1371/journal.ppat.1000335)

31. Luna C, Hoa NT, Lin H, Zhang L, Nguyen HL, Kanzok SM, Zheng L. 2006 Expression of immune responsive genes in cell lines from two different Anopheline species. *Insect. Mol. Biol.* **15**, 721–729. (doi:10.1111/j.1365-2583.2006.00661.x)

32. Boutros M, Agaisse H, Perrimon N. 2002 Sequential activation of signaling pathways during innate immune responses in *Drosophila. Dev. Cell.* **3**, 711–722. (doi:10.1016/S1534-5807(02)00325-8)

33. Souvannaseng L *et al*. 2018 Inhibition of JNK signaling in the Asian malaria vector *Anopheles stephensi* extends mosquito longevity and improves resistance to *Plasmodium falciparum* infection. *PLoS Pathog.* **14**, e1007418. (doi:10.1371/journal.ppat.1007418)

34. Silverman N, Zhou R, Erlich RL, Hunter M, Bernstein E, Schneider D, Maniatis T. 2003 Immune activation of NF-kappaB and JNK requires *Drosophila* TAK1. *J. Biol. Chem.* **278**, 48 928–48 934. (doi:10.1074/jbc.M304802200)

35. Zhuang ZH, Sun L, Kong L, Hu JH, Yu MC, Reinach P, Zang J-W, Ge B-X. 2006 *Drosophila* TAB2 is required for the immune activation of JNK and NF-kappaB. *Cell. Signal.* **18**, 964–970. (doi:10.1016/j.cellsig.2005.08.020)

36. Wong CO *et al*. 2017 Lysosomal degradation is required for sustained phagocytosis of bacteria by macrophages. *Cell Host Microbe.* **21**, 719–730. (doi:10.1016/j.chom.2017.05.002)

37. Bretscher A *et al*. 2015 The Nimrod transmembrane receptor Eater is required for hemocyte attachment to the sessile compartment in *Drosophila melanogaster. Biol. Open.* **4**, 355–363. (doi:10.1242/bio.201410595)

38. Shibata T, Sekihara S, Fujikawa T, Miyaji R, Maki K, Ishihara T, Koshiba T, Kawabata S. 2013 Transglutaminase-catalyzed protein-protein cross-linking suppresses the activity of the NF-κB-like transcription factor relish. *Sci. Signal.* **6**, ra61. (doi:10.1126/scisignal.2003970)

39. Maki K, Shibata T, Kawabata S. 2017 Transglutaminase-catalyzed incorporation of polyamines masks the DNA-binding region of the transcription factor Relish. *J. Biol. Chem.* **292**, 6369–6380. (doi:10.1074/jbc.M117.779579)

40. Yan Y, Ramakrishnan A, Estévez-Lao TY, Hillyer JF. 2022 Transglutaminase 3 negatively regulates immune responses on the heart of the mosquito, *Anopheles gambiae. Sci. Rep.* **12**, 6715. (doi:10.1038/s41598-022-10766-z)

41. Ramakrishnan A, Hillyer JF. 2022 Silencing transglutaminase genes *TGase2* and *TGase3* has infection-dependent effects on the heart rate of the mosquito *Anopheles gambiae. Insects* **13**, 582. (doi:10.3390/insects13070582)

42. Etchegaray JI, Timmons AK, Klein AP, Pritchett TL, Welch E, Meehan TL, Li C, Mccall K. 2012 Draper acts through the JNK pathway to control synchronous engulfment of dying germline cells by follicular epithelial cells. *Development* **139**, 4029–4039. (doi:10.1242/dev.082776)

43. Weavers H, Evans IR, Martin P, Wood W. 2016 Corpse engulfment generates a molecular memory that primes the macrophage inflammatory response. *Cell* **165**, 1658–1671. (doi:10.1016/j.cell.2016.04.049)

44. Frolet C, Thoma M, Blandin S, Hoffmann J, Levashina E. 2006 Boosting NF-kappa B-dependent basal immunity of *Anopheles gambiae* aborts development of *Plasmodium berghei. Immunity* **25**, 677–685. (doi:10.1016/j.immuni.2006.08.019)

45. Feng Y, Chen L, Gao L, Dong L, Wen H, Song X, Luo F, Cheng G, Wang J. 2021 Rapamycin inhibits pathogen transmission in mosquitoes by promoting immune activation. *PLoS Pathog.* **17**, e1009353. (doi:10.1371/journal.ppat.1009353)

46. Huang CY, Chou SY, Bartholomay LC, Christensen BM, Chen CC. 2005 The use of gene silencing to study the role of dopa decarboxylase in mosquito melanization reactions. *Insect. Mol. Biol.* **14**, 237–244. (doi:10.1111/j.1365-2583.2004.00552.x)

47. Paskewitz SM, Andreev O. 2008 Silencing the genes for dopa decarboxylase or dopachrome conversion enzyme reduces melanization of foreign targets in *Anopheles gambiae. Comp. Biochem. Physiol. B

Biochem. Mol. Biol. **150**, 403–408. (doi:10.1016/j.cbpb.2008.04.010)

48. Gendrin M, Zaidman-Rémy A, Broderick NA, Paredes J, Poidevin M, Roussel A, Lemaitre B. 2013 Functional analysis of PGRP-LA in *Drosophila* immunity. *PLoS ONE* **8**, e69742. (doi:10.1371/journal.pone.0069742)

49. Werner T, Liu G, Kang D, Ekengren S, Steiner H, Hultmark D. 2000 A family of peptidoglycan recognition proteins in the fruit fly *Drosophila melanogaster*. *Proc. Natl Acad. Sci. USA* **97**, 13 772–13 777. (doi:10.1073/pnas.97.25.13772)

50. Horton AA, Wang B, Camp L, Price MS, Arshi A, Nagy M, Nadler SA, Faeder JR, Luckhart S. 2011 The mitogen-activated protein kinome from *Anopheles gambiae*: identification, phylogeny and functional characterization of the ERK, JNK and p38 MAP kinases. *BMC Genomics* **12**, 574. (doi:10.1186/1471-2164-12-574)

51. Garver LS, de Almeida Oliveira G, Barillas-Mury C. 2013 The JNK pathway is a key mediator of *Anopheles gambiae* antiplasmodial immunity. *PLoS Pathog.* **9**, e1003622. (doi:10.1371/journal.ppat.1003622)

52. Kwon H, Smith R. 2019 Chemical depletion of phagocytic immune cells in *Anopheles gambiae* reveals dual roles of mosquito hemocytes in anti-*Plasmodium* immunity. *Proc. Natl Acad. Sci. USA* **116**, 14 119–14 128. (doi:10.1073/pnas.1900147116)

53. Pinto SB, Lombardo F, Koutsos AC, Waterhouse RM, McKay K, An C, Ramakrishnan C, Kafatos FC, Michel K. 2009 Discovery of *Plasmodium* modulators by genome-wide analysis of circulating hemocytes in *Anopheles gambiae*. *Proc. Natl Acad. Sci. USA* **106**, 21 270–21 275. (doi:10.1073/pnas.0909463106)

54. Baton LA, Robertson A, Warr E, Strand MR, Dimopoulos G. 2009 Genome-wide transcriptomic profiling of *Anopheles gambiae* hemocytes reveals pathogen-specific signatures upon bacterial challenge and *Plasmodium berghei* infection. *BMC Genomics* **10**, 257. (doi:10.1186/1471-2164-10-257)

55. Thomas T, De TD, Sharma P, Lata S, Saraswat P, Pandey KC, Dixit R. 2016 Hemocytome: deep sequencing analysis of mosquito blood cells in Indian malarial vector *Anopheles stephensi*. *Gene* **585**, 177–190. (doi:10.1016/j.gene.2016.02.031)

56. Bartholomay LC *et al*. 2004 Description of the transcriptomes of immune response-activated hemocytes from the mosquito vectors *Aedes aegypti* and *Armigeres subalbatus*. *Infect. Immun.* **72**, 4114–4126. (doi:10.1128/IAI.72.7.4114-4126.2004)

57. Choi YJ, Fuchs JF, Mayhew GF, Yu HE, Christensen BM. 2012 Tissue-enriched expression profiles in *Aedes aegypti* identify hemocyte-specific transcriptome responses to infection. *Insect. Biochem. Mol. Biol.* **42**, 729–738. (doi:10.1016/j.ibmb.2012.06.005)

58. Rani J *et al*. 2021 Hemocyte RNA-Seq analysis of Indian malarial vectors *Anopheles stephensi* and *Anopheles culicifacies*: from similarities to differences. *Gene* **798**, 145810. (doi:10.1016/j.gene.2021.145810)

59. Severo M *et al*. 2018 Unbiased classification of mosquito blood cells by single-cell genomics and high-content imaging. *Proc. Natl Acad. Sci. USA* **115**, E7568-E7577. (doi:10.1073/pnas.1803062115)

60. Raddi G, Barletta ABF, Efremova M, Ramirez JL, Cantera R, Teichmann SA, Barillas-Mury C, Billker O. 2020 Mosquito cellular immunity at single-cell resolution. *Science* **369**, 1128–1132. (doi:10.1126/science.abc0322)

61. Kwon H, Mohammed M, Franzén O, Ankarklev J, Smith RC. 2021 Single-cell analysis of mosquito hemocytes identifies signatures of immune cell subtypes and cell differentiation. *Elife* **10**, e66192. (doi:10.7554/eLife.66192)

62. Márkus R *et al*. 2009 Sessile hemocytes as a hematopoietic compartment in *Drosophila melanogaster*. *Proc. Natl Acad. Sci. USA* **106**, 4805–4809. (doi:10.1073/pnas.0801766106)

63. Leitão AB, Sucena É. 2015 *Drosophila* sessile hemocyte clusters are true hematopoietic tissues that regulate larval blood cell differentiation. *Elife* **4**, e06166. (doi:10.7554/eLife.06166)

64. Babcock DT, Brock AR, Fish GS, Wang Y, Perrin L, Krasnow MA, Galko MJ. 2008 Circulating blood cells function as a surveillance system for damaged tissue in *Drosophila* larvae. *Proc. Natl Acad. Sci. USA* **105**, 10 017–10 022. (doi:10.1073/pnas.0709951105)

65. Horn L, Leips J, Starz-Gaiano M. 2014 Phagocytic ability declines with age in adult *Drosophila* hemocytes. *Aging Cell* **13**, 719–728. (doi:10.1111/acel.12227)

66. Kocks C *et al*. 2005 Eater, a transmembrane protein mediating phagocytosis of bacterial pathogens in *Drosophila*. *Cell* **123**, 335–346. (doi:10.1016/j.cell.2005.08.034)

67. Moita LF, Wang-Sattler R, Michel K, Zimmermann T, Blandin S, Levashina EA, Kafatos FC. 2005 In vivo identification of novel regulators and conserved pathways of phagocytosis in *A. gambiae*. *Immunity* **23**, 65–73. (doi:10.1016/j.immuni.2005.05.006)

68. Dong Y, Das S, Cirimotich C, Souza-Neto JA, McLean KJ, Dimopoulos G. 2011 Engineered *Anopheles* immunity to *Plasmodium* infection. *PLoS Pathog.* **7**, e1002458. (doi:10.1371/journal.ppat.1002458)

69. Mantuano E, Jo M, Gonias SL, Campana WM. 2010 Low density lipoprotein receptor-related protein (LRP1) regulates Rac1 and RhoA reciprocally to control Schwann cell adhesion and migration. *J. Biol. Chem.* **285**, 14 259–14 266. (doi:10.1074/jbc.M109.085126)

70. Moita LF, Vriend G, Mahairaki V, Louis C, Kafatos FC. 2006 Integrins of *Anopheles gambiae* and a putative role of a new beta integrin, BINT2, in phagocytosis of *E. coli*. *Insect. Biochem. Mol. Biol.* **36**, 282–290. (doi:10.1016/j.ibmb.2006.01.004)

71. Rabiej VK, Pflanzner T, Wagner T, Goetze K, Storck SE, Eble JA, Weggen S, Mueller-Klieser W, Pietrzik CU. 2016 Low density lipoprotein receptor-related protein 1 mediated endocytosis of β1-integrin influences cell adhesion and cell migration. *Exp. Cell Res.* **340**, 102–115. (doi:10.1016/j.yexcr.2015.11.020)

72. Mitri C *et al*. 2009 Fine pathogen discrimination within the APL1 gene family protects *Anopheles gambiae* against human and rodent malaria species. *PLoS Pathog.* **5**, e1000576. (doi:10.1371/journal.ppat.1000576)

73. Dong Y, Simões ML, Dimopoulos G. 2020 Versatile transgenic multistage effector-gene combinations for *Plasmodium falciparum* suppression in *Anopheles*. *Sci. Adv.* **6**, eaay5898. (doi:10.1126/sciadv.aay5898)

74. Meister S, Agianian B, Turlure F, Relógio A, Morlais I, Kafatos FC, Christophides GK. 2009 *Anopheles gambiae* PGRPLC-mediated defense against bacteria modulates infections with malaria parasites. *PLoS Pathog.* **5**, e1000542. (doi:10.1371/journal.ppat.1000542)

75. Khan MB, Liew JW, Leong CS, Lau YL. 2016 Role of NF-kβ factor Rel2 during *Plasmodium falciparum* and bacterial infection in *Anopheles dirus*. *Parasit. Vectors* **9**, 525. (doi:10.1186/s13071-016-1810-0)

76. Dekmak AS, Yang X, Zu Dohna H, Buchon N, Osta MA. 2021 The route of infection influences the contribution of key immunity genes to antibacterial defense in *Anopheles gambiae*. *J. Innate Immun.* **13**, 107–126. (doi:10.1159/000511401)

77. Kambris Z, Blagborough AM, Pinto SB, Blagrove MS, Godfray HC, Sinden RE, Sinkins SP. 2010 *Wolbachia* stimulates immune gene expression and inhibits *plasmodium* development in *Anopheles gambiae*. *PLoS Pathog.* **6**, e1001143. (doi:10.1371/journal.ppat.1001143)

78. Schnitger AK, Kafatos FC, Osta MA. 2007 The melanization reaction is not required for survival of *Anopheles gambiae* mosquitoes after bacterial infections. *J. Biol. Chem.* **282**, 21 884–21 888. (doi:10.1074/jbc.M701635200)

79. Ramphul U, Garver L, Molina-Cruz A, Canepa G, Barillas-Mury C. 2015 *Plasmodium falciparum* evades mosquito immunity by disrupting JNK-mediated apoptosis of invaded midgut cells. *Proc. Natl Acad. Sci. USA* **112**, 1273–1280. (doi:10.1073/pnas.1423586112)

80. Peirce MJ *et al*. 2020 JNK signaling regulates oviposition in the malaria vector *Anopheles gambiae*. *Sci. Rep.* **10**, 14344. (doi:10.1038/s41598-020-71291-5)

81. Nsango S *et al*. 2013 AP-1/Fos-TGase2 axis mediates wounding-induced *Plasmodium falciparum* killing in *Anopheles gambiae*. *J. Biol. Chem.* **288**, 16 145–16 154. (doi:10.1074/jbc.M112.443267)

82. Chowdhury A, Modahl C, Tan S, Xiang B, Misse D, Vial T, Kini RM, Pompon JF. 2020 JNK pathway restricts DENV2, ZIKV and CHIKV infection by activating complement and apoptosis in mosquito salivary glands. *PLoS Pathog.* **16**, e1008754. (doi:10.1371/journal.ppat.1008754)

83. Williams MJ, Wiklund ML, Wikman S, Hultmark D. 2006 Rac1 signalling in the *Drosophila* larval cellular

immune response. *J. Cell Sci.* **119**(Pt 10), 2015–2024. (doi:10.1242/jcs.02920)

84. Zettervall CJ, Anderl I, Williams MJ, Palmer R, Kurucz E, Ando I, Hultmark D. 2004 A directed screen for genes involved in *Drosophila* blood cell activation. *Proc. Natl Acad. Sci. USA* **101**, 14 192–14 197. (doi:10.1073/pnas.0403789101)

85. Ma L, Liu L, Zhao Y, Yang L, Chen C, Li Z, Lu Z. 2020 JNK pathway plays a key role in the immune system of the pea aphid and is regulated by microRNA-184. *PLoS Pathog.* **16**, e1008627. (doi:10.1371/journal.ppat.1008627)

86. Macdonald JM, Doherty J, Hackett R, Freeman MR. 2013 The c-Jun kinase signaling cascade promotes glial engulfment activity through activation of draper and phagocytic function. *Cell Death Differ.* **20**, 1140–1148. (doi:10.1038/cdd.2013.30)

87. Manaka J, Kuraishi T, Shiratsuchi A, Nakai Y, Higashida H, Henson P, Nakanishi Y. 2004 Draper-mediated and phosphatidylserine-independent phagocytosis of apoptotic cells by *Drosophila* hemocytes/macrophages. *J. Biol. Chem.* **279**, 48 466–48 476. (doi:10.1074/jbc.M408597200)

88. Evans IR, Rodrigues FS, Armitage EL, Wood W. 2015 Draper/CED-1 mediates an ancient damage response to control inflammatory blood cell migration in vivo. *Curr. Biol.* **25**, 1606–1612. (doi:10.1016/j.cub.2015.04.037)

89. Levashina EA, Moita LF, Blandin S, Vriend G, Lagueux M, Kafatos FC. 2001 Conserved role of a complement-like protein in phagocytosis revealed by dsRNA knockout in cultured cells of the mosquito, *Anopheles gambiae*. *Cell* **104**, 709–718. (doi:10.1016/S0092-8674(01)00267-7)

90. Nagaosa K *et al*. 2011 Integrin βv-mediated phagocytosis of apoptotic cells in *Drosophila* embryos. *J. Biol. Chem.* **286**, 25 770–25 777. (doi:10.1074/jbc.M110.204503)

91. Chakrabarti S, Dudzic JP, Li X, Collas EJ, Boquete JP, Lemaitre B. 2016 Remote control of intestinal stem cell activity by haemocytes in *Drosophila*. *PLoS Genet.* **12**, e1006089. (doi:10.1371/journal.pgen.1006089)

92. Qiu P, Pan PC, Govind S. 1998 A role for the *Drosophila* Toll/Cactus pathway in larval hematopoiesis. *Development* **125**, 1909–1920. (doi:10.1242/dev.125.10.1909)

93. Chiu H, Ring BC, Sorrentino RP, Kalamarz M, Garza D, Govind S. 2005 dUbc9 negatively regulates the Toll-NF-kappa B pathways in larval hematopoiesis and drosomycin activation in *Drosophila*. *Dev. Biol.* **288**, 60–72. (doi:10.1016/j.ydbio.2005.08.008)

94. Hernández-Martínez S, Sánchez-Zavaleta M, Brito K, Herrera-Ortiz A, Ons S, Noriega FG. 2017 Allatotropin: a pleiotropic neuropeptide that elicits mosquito immune responses. *PLoS ONE* **12**, e0175759. (doi:10.1371/journal.pone.0175759)

95. Destalminil-Letourneau M, Morin-Poulard I, Tian Y, Vanzo N, Crozatier M. 2021 The vascular niche controls *Drosophila* hematopoiesis via fibroblast growth factor signaling. *Elife* **10**, e64672. (doi:10.7554/eLife.64672)

96. Dragojlovic-Munther M, Martinez-Agosto JA. 2013 Extracellular matrix-modulated Heartless signaling in *Drosophila* blood progenitors regulates their differentiation via a Ras/ETS/FOG pathway and target of rapamycin function. *Dev. Biol.* **384**, 313–330. (doi:10.1016/j.ydbio.2013.04.004)

97. Cevik D, Acker M, Michalski C, Jacobs JR. 2019 Pericardin, a *Drosophila* collagen, facilitates accumulation of hemocytes at the heart. *Dev. Biol.* **454**, 52–65. (doi:10.1016/j.ydbio.2019.06.006)

98. Blandin S, Levashina EA. 2004 Thioester-containing proteins and insect immunity. *Mol. Immunol.* **40**, 903–908. (doi:10.1016/j.molimm.2003.10.010)

99. Bou AR, Hetru C, Troxler L, Doucet D, Ferrandon D, Matt N. 2011 Analysis of thioester-containing proteins during the innate immune response of *Drosophila melanogaster*. *J. Innate Immun.* **3**, 52–64. (doi:10.1159/000321554)

100. Somogyi K, Sipos B, Pénzes Z, Kurucz E, Zsámboki J, Hultmark D, Ando I. 2008 Evolution of genes and repeats in the Nimrod superfamily. *Mol. Biol. Evol.* **25**, 2337–2347. (doi:10.1093/molbev/msn180)

101. Nishide Y, Kageyama D, Yokoi K, Jouraku A, Tanaka H, Futahashi R, Fukatsu T. 2019 Functional crosstalk across IMD and Toll pathways: insight into the evolution of incomplete immune cascades. *Proc. R. Soc. B* **286**, 20182207. (doi:10.1098/rspb.2018.2207)

102. Salcedo-Porras N, Guarneri A, Oliveira PL, Lowenberger C. 2019 *Rhodnius prolixus*: Identification of missing components of the IMD immune signaling pathway and functional characterization of its role in eliminating bacteria.

PLoS ONE **14**, e0214794. (doi:10.1371/journal.pone.0214794)

103. Mesquita RD *et al*. 2015 Genome of *Rhodnius prolixus*, an insect vector of Chagas disease, reveals unique adaptations to hematophagy and parasite infection. *Proc. Natl Acad. Sci. USA* **112**, 14 936–14 941. (doi:10.1073/pnas.1506226112)

104. Gerardo NM *et al*. 2010 Immunity and other defenses in pea aphids, *Acyrthosiphon pisum*. *Genome Biol.* **11**, R21. (doi:10.1186/gb-2010-11-2-r21)

105. Glenn JD, King JG, Hillyer JF. 2010 Structural mechanics of the mosquito heart and its function in bidirectional hemolymph transport. *J. Exp. Biol.* **213**, 541–550. (doi:10.1242/jeb.035014)

106. Hillyer JF, Christensen BM. 2002 Characterization of hemocytes from the yellow fever mosquito, *Aedes aegypti*. *Histochem. Cell Biol.* **117**, 431–440. (doi:10.1007/s00418-002-0408-0)

107. Dobin A, Davis CA, Schlesinger F, Drenkow J, Zaleski C, Jha S, Batut P, Chaisson M, Gingeras TR. 2013 STAR: ultrafast universal RNA-seq aligner. *Bioinformatics* **29**, 15–21. (doi:10.1093/bioinformatics/bts635)

108. Giraldo-Calderón GI *et al*. 2015 VectorBase: an updated bioinformatics resource for invertebrate vectors and other organisms related with human diseases. *Nucleic Acids Res.* **43**(Database issue), D707–D713. (doi:10.1093/nar/gku1117)

109. Love MI, Huber W, Anders S. 2014 Moderated estimation of fold change and dispersion for RNA-seq data with DESeq2. *Genome Biol.* **15**, 550. (doi:10.1186/s13059-014-0550-8)

110. Everaert C, Luypaert M, Maag JLV, Cheng QX, Dinger ME, Hellemans J, Mestdagh P. 2017 Benchmarking of RNA-sequencing analysis workflows using whole-transcriptome RT-qPCR expression data. *Sci. Rep.* **7**, 1559. (doi:10.1038/s41598-017-01617-3)

111. League GP, Estévez-Lao TY, Yan Y, Garcia-Lopez VA, Hillyer JF. 2017 *Anopheles gambiae* larvae mount stronger immune responses against bacterial infection than adults: evidence of adaptive decoupling in mosquitoes. *Parasit. Vectors* **10**, 367. (doi:10.1186/s13071-017-2302-6)

112. Yan Y, Sigle LT, Rinker DC, Estévez-Lao TY, Capra JA, Hillyer JF. 2022 The immune deficiency and c-Jun N-terminal kinase pathways drive the functional integration of the immune and circulatory systems of mosquitoes. Figshare. (doi:10.6084/m9.figshare.c.6167568)